Journal of the mechanical behavior of biomedical materials 73 (2017) 38–49

Contents lists available at ScienceDirect

Journal of the Mechanical Behavior of Biomedical Materials

journal homepage: www.elsevier.com/locate/jmbbm

Spines of the porcupine fish: Structure, composition, and mechanical properties

Frances Y. Su[a,*], Eric A. Bushong[b], Thomas J. Deerinck[b], Kyungah Seo[a], Steven Herrera[c], Olivia A. Graeve[a,d], David Kisailus[c], Vlado A. Lubarda[d,e], Joanna McKittrick[a,d]

[a] Materials Science and Engineering Program, University of California, San Diego, 9500 Gilman Dr., La Jolla, CA 92093-0418, USA
[b] National Center for Microscopy and Imaging Research, University of California, San Diego, 9500 Gilman Dr., La Jolla, CA 92093-0608, USA
[c] Chemical and Environmental Engineering, University of California, Riverside, 900 University Ave., Riverside, CA 92521, USA
[d] Mechanical and Aerospace Engineering, University of California, San Diego, 9500 Gilman Dr., La Jolla, CA 92093-0411, USA
[e] Department of NanoEngineering, University of California, San Diego, 9500 Gilman Dr., La Jolla, CA 92093-0448, USA

ARTICLE INFO

Keywords:
Porcupine fish
X-ray microscopy
Nanoindentation
Microstructure
Mechanical properties

ABSTRACT

This paper explores the structure, composition, and mechanical properties of porcupine fish spines for the first time. The spine was found to be composed of nanocrystalline hydroxyapatite, protein (collagen), and water using X-ray diffraction, energy-dispersive X-ray spectroscopy, and thermogravimetric analysis. Microstructures have mineralized fibrillar sheets in the longitudinal direction and in a radial orientation in the transverse direction that were observed using light and electron microscopy. Based on the images, the hierarchical structure of the spine shows both concentric and radial reinforcement. Mechanical properties were obtained using cantilever beam and nanoindentation tests. A tapered cantilever beam model was developed and compared to that of a uniform cantilever beam. The tapered beam model showed that while the stresses experienced were similar to those of the uniform beam, the location of the maximum stress was near the distal region of the beam rather than at the base, which allows the porcupine fish to conserve energy and resources if the spine is fractured.

1. Introduction and background

Spines are stiff, tapered structures that protrude from an organism. They are found in mammals (e.g. porcupine, echidna, and hedgehog), plants (e.g. cacti and rose), insects, reptiles, birds, echinoderms, and fish. While spines can be used offensively, for instance in bees and wasps, many organisms use spine structures as a form of defense. Organisms that use spines for defense include porcupines, hedgehogs, cacti, and sea urchins. Spines are used to deter predators by piercing and irritating.

Spine structures can be made of a variety of biological materials. Sea urchin (Fig. 1a) spines are composed of magnesium calcite (Berman et al., 1990; Moureaux et al., 2010); lionfish (Fig. 1b) dorsal spines (Bassett, 1917; Bowes and Murray, 1935; Halstead et al., 1955); and stingray (Fig. 1c) stings are composed of mineralized collagen (Halstead and Modglin, 1950; Ocampo et al., 1953); spines and quills found in hedgehogs, porcupines (Fig. 1d), and echidnas (Fig. 1e) are made of keratin (Martin et al., 2015; Vincent and Owers, 1986); cactus (Fig. 1f) spines are made almost equal parts of crystalline cellulose and amorphous hemicellulose, both of which are polysaccharides (Gindl-Altmutter and Keckes, 2012; Malainine et al., 2003). Meanwhile, scorpion (Fig. 1g), bee (Fig. 1h), and wasp stingers are made of the polysaccharide chitosan (Zhao et al., 2016; Zhao et al., 2015).

Many spine structures, including the previously mentioned scorpion stinger, are known to be functionally graded materials, which have gradients in composition or structural characteristics. The squid beak (Miserez et al., 2008), ancient fish armor (Bruet et al., 2008), and spider fang (Bar-On et al., 2014) all exhibit compositional gradients resulting in a gradual transition in Young's modulus. Functionally graded materials have been found to reduce deformation and damage at material surfaces and dissipate stress by transitioning to a more compliant material (Bechtle et al., 2010; Liu et al., 2016; Pompe et al., 2003).

It is also important to note the multifunctionality that is intrinsic to biological materials. Spines can be useful to an organism for a variety of reasons. For example, in addition to protection, the cactus uses its spines, to prevent water loss in its native desert habitat. Hedgehogs use their quills not only to deter predators, but also to absorb energy when

* Corresponding author.
E-mail address: fysu@eng.ucsd.edu (F.Y. Su).

http://dx.doi.org/10.1016/j.jmbbm.2017.02.029
Received 27 September 2016; Received in revised form 4 February 2017; Accepted 26 February 2017
Available online 28 February 2017
1751-6161/

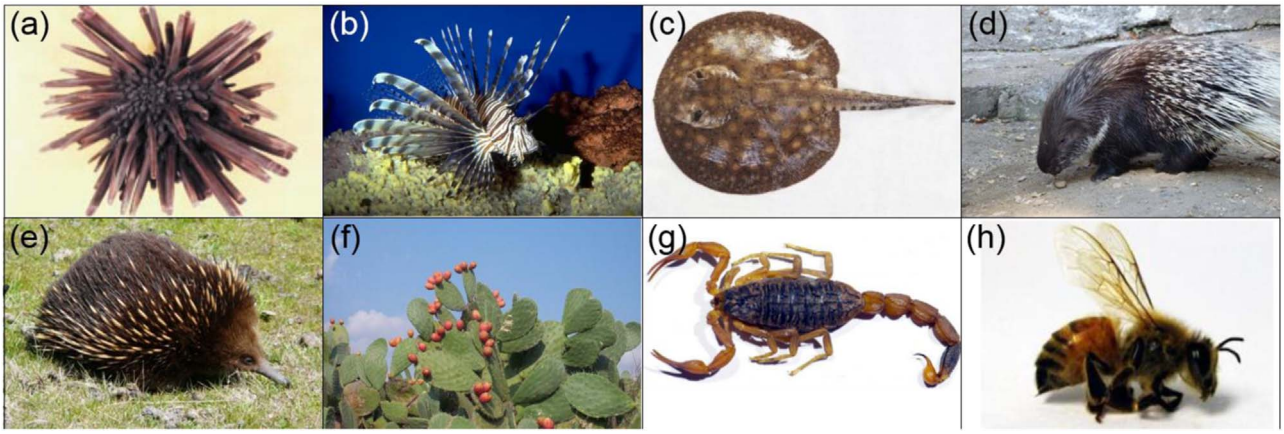

Fig. 1. Various organisms with spine structures. (a) Sea urchin (Su et al., 2000), (b) lionfish (Corsi and Corsi, 2001), (c) stingray (Pedroso et al., 2007), (d) porcupine (Tonge, 2014), (e) echidna (Tonge, 2013), (f) cactus (Rignanese, 2005), (g) scorpion (Zhao et al., 2016), and (h) honey bee (Zhao et al., 2015). Figures are adapted from cited sources.

they fall from high places (Vincent and Owers, 1986). The lionfish, stingray, bee, wasp, and scorpion all use venom to supplement their stings.

Porcupine fish belong to a family within the order Tetraodontiformes called Diodontidae (Santini et al., 2013). While the order Tetradontiformes is an extremely diverse group that includes the boxfish and triggerfishes, the porcupine fish is most closely related to the families Tetraodontidae and Molidae, which include pufferfish and ocean sunfish, respectively (Santini et al., 2013). Porcupine fish are preyed upon by pelagic predators including tuna, dolphinfish, and wahoo (Aquarium of the Pacific, 2015). Once porcupine fish reach the adult stage and become too large to swallow, the number of predators decreases significantly. The main predator of the adult porcupine fish is the tiger shark.

To protect themselves, porcupine fish, like their pufferfish relatives, inflate their bodies up to three times their original volume (Brainerd, 1994). During inflation, water or air is pumped into the stomach. In addition to inflation, porcupine fish also have long spines across their bodies that are erectile when the fish inflates (Leis, 2006). These spines are actually modified scales and serve to both irritate the predator and increase the effective volume of the porcupine fish, making it harder for predators to swallow.

Apart from general observations, little to no work has been done on the composition and microstructure of the porcupine fish spine. However, some work has been done to understand the spine structure in the family Tetraodontidae. Hertwig et al. (1992) observed that the dermal spines in *Tetraodon steindachneri* have bilateral symmetry and a laminated longitudinal cross-section. The spines of the *T. steindachneri* and *Takifugu obscurus* can be stained using alizarin red-S, a histological dye that indicates the presence of calcium (Byeon et al., 2011; Hertwig et al., 1992). Of note, these spines have a dense outer layer of collagen around a mineralized core (Hertwig et al., 1992), as well as numerous concentric circles in the transverse cross-section of the spines (Byeon et al., 2011).

The composition of porcupine fish spines is largely unknown, since alizarin red only signifies the presence of calcium, but does not specify whether the spines contain calcium carbonate, hydroxyapatite, or both minerals. As modified scales, the spines can be expected to be compositionally similar to that of other fish scales, comprising highly aligned type I collagen, calcium phosphate (e.g. hydroxyapatite and tricalcium phosphate), and in some cases, calcium carbonate (Ehrlich, 2015; Lin et al., 2011; Zylberberg et al., 1992). Sire et al. (2009) noted that the dermal plates in tetraodontiforms are composed of only bone. However, the order Tetraodontiformes is so diverse in morphology that it is unlikely that every modified scale across the order is compositionally identical.

In the porcupine fish, Brainerd (1994) identified three different regions of the spine: the spinous process, the lateral processes, and the axial process. Leis (1978) referred to these regions as the spine shaft, the lateral arms of the base, and shaft extension, respectively. Spines generally have bilateral symmetry with two lateral processes, one spinous process, and one axial process.

This work aims to characterize the composition, structure and mechanical properties of the spines from two porcupine fish, *Diodon holocanthus* (Long-spine) and *Diodon hystrix* (Spot-fin). The spines must be able to withstand the force of a predator's jaw to maintain structural integrity. There are two main hypotheses we have explored: (1) the composition of the spines will be similar to that of other scales, meaning that the spines will likely contain collagen and calcium phosphate mineral, and (2) the morphology and consequent mechanical properties of the spines help prevent spine fracture.

2. Materials and methods

One of each *D. holocanthus* (Museum ID: SIO 65–679) and *D. hystrix* (Museum ID: SIO H52-415) (Fig. 2) were received from the Scripps Institution of Oceanography. Samples had been fixed with 10% formalin and post-fixed in 50% isopropyl alcohol and deionized water. Spines were extracted from the right lateral side of the fish using a

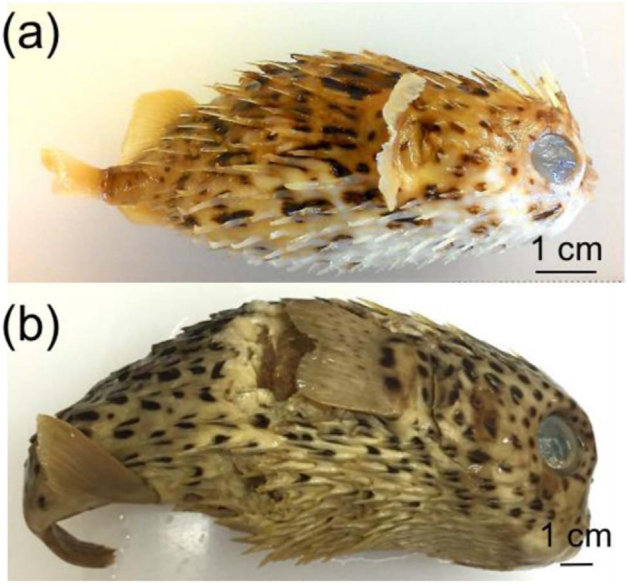

Fig. 2. Photographs of the specimens used in this study, (a) *Diodon holocanthus* (slender-bodied long-spine porcupine fish) and (b) *Diodon hystrix* (round-bodied spot-fin porcupine fish) samples received from the Scripps Institution of Oceanography.

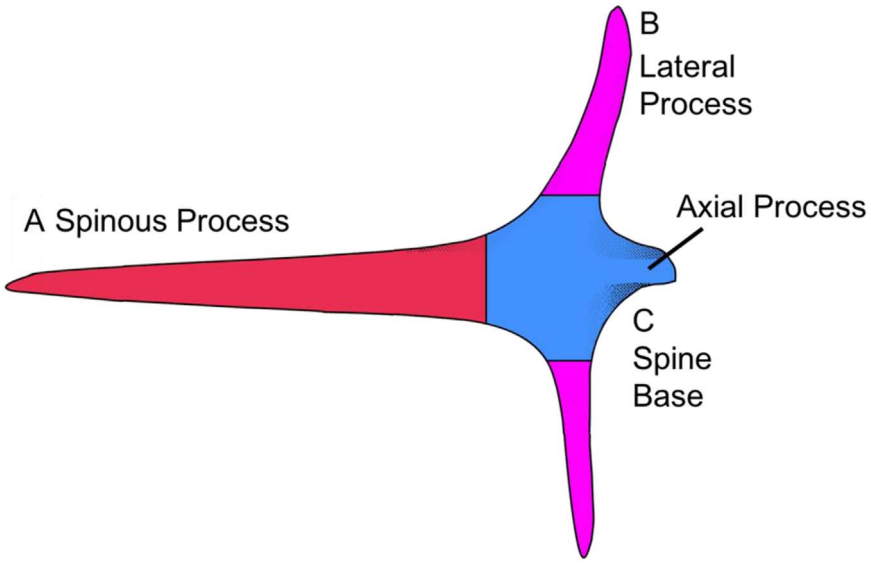

Fig. 3. Colorized schematic diagram of a porcupine fish spine where A is the spinous process (red), B are the two lateral processes (pink), and C is the spine base (blue), which includes the axial process and the connection between sections A and B.

scalpel and surgical scissors to cut away skin and other connective tissue until the spine could be pried loose. Spines of both species were initially compared using optical microscopy and found to have the same structure as shown in Supplementary Materials, therefore both spines were used for imaging and compositional analysis while only *D. holocanthus* spines were used for mechanical testing for consistency. Individual spines were stored in 50% isopropyl alcohol and deionized water.

Deproteinization was achieved by placing the spine in a 2.6% sodium hypochlorite solution for two days. The solution was changed each day. Samples were then rinsed gently with deionized water to remove excess sodium hypochlorite solution. After rinsing, samples were dehydrated using hexamethyldisilazane.

2.1. Compositional analysis

X-ray diffraction (XRD) was performed on one *D. hystrix* spine sample that was deproteinized. The sample was split into sections A, B, and C as shown in Fig. 3, and ground to a powder using a mortar and pestle. XRD was then performed on the powders (Bruker D2 Phaser, Bruker, Billerica, MA, USA) using CuKα radiation. Pattern analysis was completed using DIFFRACplus software (Bruker, Billerica, MA, USA).

XRD patterns were matched using standard data from a PDF card. The crystallite size was found using the Scherrer equation

$$D=\frac{0.94\lambda}{\beta cos\theta} \quad (1)$$

where D is the average crystallite size, λ is the X-ray wavelength (0.15406 nm), β is the full width at half of the maximum intensity, and θ is the Bragg angle. Three of the peaks with highest intensity were used to calculate the average crystallite size.

Six samples of *D. holocanthus* spines prepared for thermogravimetric analysis (TGA) (SDT Q600 Simultaneous TGA/DSC, TA Instruments, New Castle, DE, USA) were first step-wise rehydrated by placing the samples in solutions of 25%, 12.5%, and 0% isopropyl alcohol and deionized water for 10 minutes in each solution. Samples were then put in deionized water again and left overnight. Samples were cut into three sections A, B, and C (Fig. 3) with excess water removed by dabbing with a tissue before testing. Samples were then heated from room temperature to 800°C at a rate of 10°C/min in air. Values of mass were taken from the temperature closest to those given by Bigi et al. (1991). The percentage of mass loss was calculated by dividing leftover mass by original mass of the sample. All calculated values are given as mean ± standard deviation.

Fourier transform infrared spectroscopy (FTIR) was used to determine whether collagen was the structural protein present in the *D. holocanthus* spine. An Agilent Cary 680 spectrometer (Agilent Technologies, Inc., La Jolla, CA, USA) was used in reflection mode with a KBr beamsplitter, a mid-IR source, and a mercury cadmium telluride detector in nitrogen atmosphere. The spot size was 100 μm and the frequency range tested was from 700 to 4000 cm^{-1}.

2.2. Microstructural characterization

For x-ray microscopy (XRM) the whole *D. holocanthus* sample was kept in a jar of 50% isopropyl alcohol and deionized water and then imaged (Skyscan 1076 μ-CT scanner, Bruker, Kontich, Belgium) with a voxel size of 12.56 μm and an acceleration voltage of 100 kV, resulting in 2,187 projection images. Spine samples were first rehydrated, stained with osmium tetroxide, dehydrated, and embedded in Spurrs resin. Spurrs resin was used because of its low viscosity and ability to infiltrate mineralized samples better than other resins. Samples were then imaged (Xradia 510 Versa, ZEISS, Jena, Germany) with a voxel size of 11.02 μm and an acceleration voltage of 40 kV for 3,200 projection images. XRM results were processed using Amira® software (FEI, Oregon, USA).

In preparation for scanning electron microscopy (SEM) and energy dispersive X-ray spectroscopy (EDS), *D. hystrix* spines were step-wise dehydrated with 75%, 90%, 95%, and 100% isopropyl alcohol for 10 minutes each. Samples were then critical point dried using a critical point dryer (Autosamdri-815, Tousimis, Rockville, MD, USA) or chemically dried using hexamethyldisilazane (HMDS). Samples were sputter coated with iridium at 85 μA for 7 seconds to reduce charging using a sputter coater (Emitech K575X, Quorum Technologies Ltd, East Sussex, UK). Spines were then imaged using an environmental SEM (FEI/Philips XL-30, FEI, Hillsboro, OR, USA). EDS was performed using an ultra-high resolution SEM (FEI SFEG, FEI, Hillsboro, OR, USA).

Spine samples used for histology were first rehydrated and stained with osmium tetroxide. After staining, samples were washed and stepwise dehydrated with ethanol and then acetone. Samples were then embedded in Spurrs resin and sectioned using a microtome (Leica Ultracut UCT Ultramicrotome, Leica Microsystems, Wetzlar, Germany) into 250 nm slices and 80 nm slices for histology and transmission

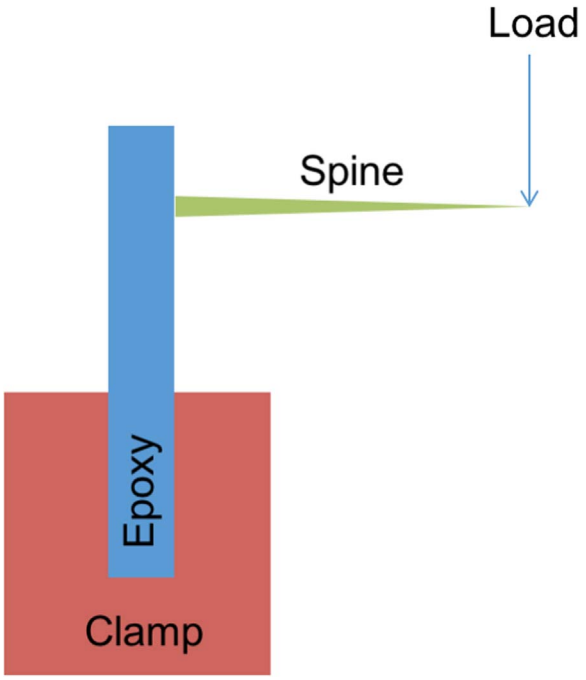

Fig. 4. Schematic of spine cantilever beam test. The clamp is 25.5 mm in width, epoxy is ~3.5 mm in thickness and 8 mm in width. Spines are ~5–6 mm in length.

electron microscopy (TEM), respectively. Histology samples were stained with Toluidine blue and then imaged with an optical microscope (Nikon Eclipse E600FN, Nikon, Tokyo, Japan) using a digital single-lens reflex camera (Nikon D300 DX, Nikon, Tokyo, Japan). TEM samples were placed on a copper grid, stained with Sato lead to increase contrast, and imaged (JEOL 1200EX, JEOL Ltd. Tokyo, Japan).

2.3. Mechanical properties

To prepare samples for cantilever beam testing, spines were rehydrated with the same method as used for TGA and the spine base was embedded in a two-part epoxy (in EpoxiCure 2, Buehler, Lake Bluff, IL, USA) with the spinous process protruding from the epoxy. The samples were left to cure at room temperature overnight and then sanded down to dimensions to fit in the mechanical testing clamps that were 7.7 mm in thickness, 25.6 mm in width, and 25.4 mm in height. An instrumented load frame (Instron 3342, Instron, Massachusetts, USA) was used to perform cantilever beam tests with a 50 N load cell with the setup shown in Fig. 4. The rate of crosshead displacement was 0.003 mm/s.

Nanoindentation was performed on dried samples of *D. holocanthus* spines using a nanoindenter (TI-950 Tribo-Indenter, Hysitron Inc., Minneapolis, MN, USA). Samples were first embedded in epoxy and the surface was polished to a mirror finish using 0.05 µm diamond polishing media. A nanoindentation map of the spinous process longitudinal cross-section was created using a cube corner probe tip with indentation depth of 300 nm, 75 µm spacing between indents, and a trapezoidal 10-10-10 s load-hold-unloading displacement function. Nanoindentation data was analyzed using the Oliver-Pharr method (Oliver and Pharr, 1992).

3. Results and discussion

The *D. holocanthus* specimen had a body length of ~9 cm and the number of spines on the fish was ~222. The *D. hystrix* specimen had a body length of ~19 cm with ~410 spines. Leis (1978) counted the number of spines in certain areas and rows of spines in other areas, but did not report overall number of spines for fish. The difference in the number of spines may reflect the size difference of the two species, where *D. hystrix* are ~40 cm (Sanches, 1991) and *D. holocanthus* are ~15 cm (Prado et al., 2004). *D. holocanthus* spines were ~6.4 mm in length and ~1 mm in diameter.

Table 1
Comparison of elemental composition between spine base (center) and spinous process from energy dispersive X-ray spectroscopy analysis given in atomic percentage. Fig. 3 shows the locations of (A) and (B).

Element	(A) Spine base (at%)	(B) Spinous process (at%)
C	57.9	16.3
O	29.7	40.1
P	12.1	25.3
Ca	0.4	23.9

3.1. Compositional analysis

EDS was used to identify elements in two regions of the spine: the spinous process and the central part of the spine base. Values in Table 1 were calculated with the Iridium Ultra software (eumeX Instrumentebau GmbH, Heidenrod, Germany) using the ZAF algorithm, which calculates the mass and atomic percentages using the area under the spectroscopy curves, atomic number, absorbance, and fluorescence of the sample. From the high carbon content and extremely low calcium content, it is reasonable to assume that the center of the spine base is mostly, if not completely, composed of organic material. The composition of the spinous process implies that it has a mixture of organic and mineral material. The organic component of the porcupine fish spines is most likely collagen, which is found in many other fish spines (Ikoma et al., 2003b; Zhu et al., 2012; Zylberberg et al., 1992). Given the high atomic percentage of phosphorus in the region with high concentrations of calcium, the porcupine fish spine likely contains calcium phosphate mineral in the form of hydroxyapatite ($Ca_{10}(PO_4)_6(OH)_2$), β tricalcium phosphate (β –TCP) ($Ca_3(PO_4)_2$), or a mixture of both based on previous work on fish bone (Hamada et al., 1995; Urist, 1961) and scales (Ikoma et al., 2003a; Meinke et al., 1979).

XRD was used to confirm the presence of hydroxyapatite in the porcupine fish spine. As seen in Fig. 5, the peaks of each region of the spine match the standard XRD pattern for hydroxyapatite (PDF 01–076-0694) (Elliott et al., 1973) and are consistent with those seen in other scales (Ikoma et al., 2003a; Lin et al., 2011). The broad peaks in the pattern indicate that the sample is nanocrystalline. Crystallite sizes

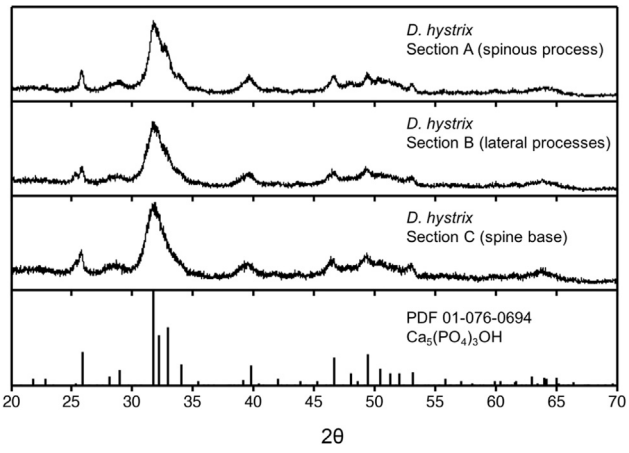

Fig. 5. X-ray diffraction pattern of different sections of the *D. hystrix* spine. From top to bottom: XRD pattern for sections A, B, and C of the spine (Fig. 3) and the standard XRD pattern for monoclinic hydroxyapatite powder diffraction file number 01–076-0694 (Elliott et al., 1973).

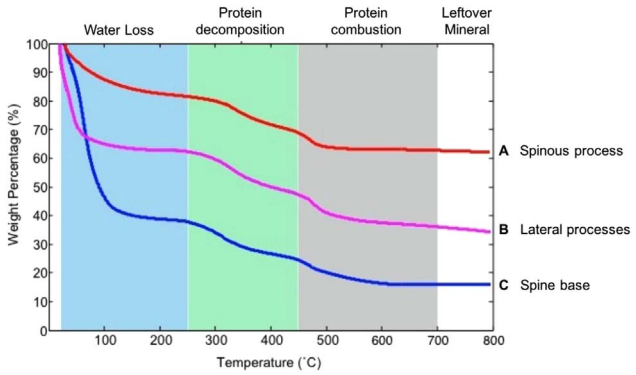

Fig. 6. Representative thermogravimetric curves for different sections of *D. holocanthus* spines from sections A, B, and C (Fig. 3). Water loss occurred between room temperature to approximately 250°C. Collagen decomposition and combustion occurred from 250°C to 700°C. The remaining mass after the sample has reached ~700°C is the mineral.

were calculated with the Scherrer equation (Eqn. (1)) using peaks (221), ($\bar{3}\bar{8}0$), and (242) since they were the most pronounced peaks in the spectra. The average values for the crystallite sizes are ~20.1 nm, ~20.4 nm, and ~20.8 nm for the spinous process, lateral processes, and spine base, respectively. Due to the broad peaks of the material used, it is difficult to say whether β –TCP is present in the porcupine fish spine in small quantities. It is of note that while some fish scales (e.g., crappie and bass) have been known to contain calcite (Ehrlich, 2015), no calcite was found in the porcupine fish spines.

TGA revealed that each section of the spine has a different composition of mineral, protein and water. Fig. 6 shows three representative TGA curves for the spinous process, the lateral processes, and the spine base, which includes the axial process. Mass loss between room temperature and 250°C corresponds to water loss (Bigi et al., 1991; Janković et al., 2009) and mass loss from 250°C to 700°C corresponds to collagen decomposition and subsequent combustion (Bigi et al., 1991). Compositions by weight percentage of sections A (spinous process), B (lateral process), and C (axial process) are summarized in Table 2, where values are given as mean ± standard deviation. Excess tissue was difficult to completely remove from sections B and C resulting in variations in protein and water content. Section C has the largest amount of protein and water, while section A has the most mineral.

3.2. Meso- and micro-structural characterization

X-ray microscopy images from a *D. holocanthus* specimen are shown in Fig. 7a,b. The spines create a layer of subdermal armor as a result of lateral processes that extend beneath one another (Fig. 7a). Fig. 7c-g shows that each spine is composed of three distinct parts and corroborates previous observations (Brainerd, 1994). The axial process (C) is markedly shorter than the lateral processes (B), which allows the spine to be erected during inflation (Fig. 7c-e). A thin layer of less dense tissue surrounding the dense spine mineral can be seen, which was observed by Hertwig et al. (1992) for the *T. steindachneri* spine. A density gradient can also be seen on the spine, where the section A is denser than sections B and C (Fig. 7e). This confirms the results from TGA, since the more mineralized regions are denser. The dorsal and ventral views of the spine (Fig. 7f,g) show that the spine transitions from a circular to a triangular cross-section from the distal to proximal end.

Table 2
Thermogravimetric analysis of *D. holocanthus* spines in sections A. B and C (Fig. 3). Values of weight percentage are given as average ± standard deviation.

	A	B	C
	(wt%)	(wt%)	(wt%)
Water	18 ± 1.2	36 ± 15.2	59 ± 6.2
Protein	19 ± 0.6	25 ± 4.2	23 ± 2.7
Mineral	63 ± 1.4	39 ± 15.0	17 ± 7.2

SEM was used to observe the mesostructure from a *D. hystrix* freeze-fractured spine. Fig. 8a shows the fractured spine surface, where the distal end of the spine is pointing toward the right. The location of the fracture is shown in the inset image. From the fracture surface a layered structure can be observed, and each layer was subsequently imaged in more detail. Fig. 8b shows the outer connective tissue, which attaches the spine to the skin. The core (Fig. 8c) was found to be mineralized using XRD and EDS carried out on the spine longitudinal cross-section in Section 3.1. The step-like fracture surface of the core implies a layered internal structure. Finally, a porous and fibrillar layer is sandwiched between the mineral core and connective tissue, shown in Fig. 8d. This layer is composed of smaller fibrils shown in Fig. 8e, and the fibrils form a porous sheet of ~2 μm thickness with fibrillar strips of ~2 μm joined by fibrillar bridges. A structure similar to the porous, fibrillar layer is found in the scales of the sea bream *Pagrus major* as described in Ikoma et al. (2003a). An overall schematic diagram of the spine layers is shown in Fig. 8f.

Fibrils identified in the proximal end of the spine have banding that indicate the presence of collagen (Fig. 9a) with *d*-spacing measuring ~67 nm. FTIR spectra (Fig. 9b) taken along the longitudinal cross-section of the spine confirmed that these fibrils are composed of collagen, which has an amid I peak at ~1650 cm^{-1}, amide II peak at ~1560 cm^{-1}, and a three-peak cluster centered at ~1245 cm^{-1} (Vidal and Mello, 2011). The polished longitudinal cross-section of the distal end of the spine (Fig. 9c) shows that the material is longitudinally aligned. Deproteinization was used to determine which areas of the spine are mineralized and the mineral structure in those areas. Previous studies have shown that bone deproteinized with diluted NaOCl solution retained the structure of the mineral after treatment while removing collagen (Chen et al., 2011; Chen and McKittrick, 2011). After deproteinization, a mineralized sheet with mineralized bridges joining the sheet together was observed (Fig. 9d), verifying that the fibrils are mineralized collagen.

In the transverse direction, stained histological images show circumferential connective tissue and the porous, fibrillar layer, with a core mineralized region that has a radial pattern (Fig. 10a), corroborating what was seen by SEM. Toluidine blue stains acidic components such as nucleic acids and proteins including collagen. The dark core, radial lines are mineralized collagen. Mineralized, fibrillar sheets have been observed in a variety of fish scales and dorsal spines, including those of the goldfish (Zylberberg and Nicolas, 1982), cobitid fish (Reddy, 2006), and chondrichthyan fishes (i.e., dogfishes, horn sharks, and ghost sharks) (Clarke and Irvine, 2006). Using back-scattered electron microscopy, a concentric ring pattern was also seen in the transverse cross-section (Fig. 9b). These growth rings have widths that range from 2 to 7.5 μm per ring. Growth rings are commonly seen in many other fish scales and have been often used to distinguish the age of a fish by correlating mass increase per year with width of growth rings (de Albuquerque et al., 2011). However, no work has been done to determine the age of porcupine fish using spine growth rings.

Fig. 10c is a TEM image of spine transverse cross-section and shows that the radiating mineralized, fibrillar sheets that have a thickness of ~2 μm, as well as bridges that periodically connect these sheets. Layers of radially aligned, unmineralized collagen fibrils alternate between these sheets. The growth front of the spine can also be observed. The thickness of the mineralized, fibrillar sheets matches the thickness of the fibrillar strips observed in SEM (Fig. 8e). Observing that the mineralized core is both longitudinally aligned and radially symmetric, one can conclude that there are porous sheets of longitudinally aligned, mineralized collagen that are arranged radially with respect to the transverse cross-section.

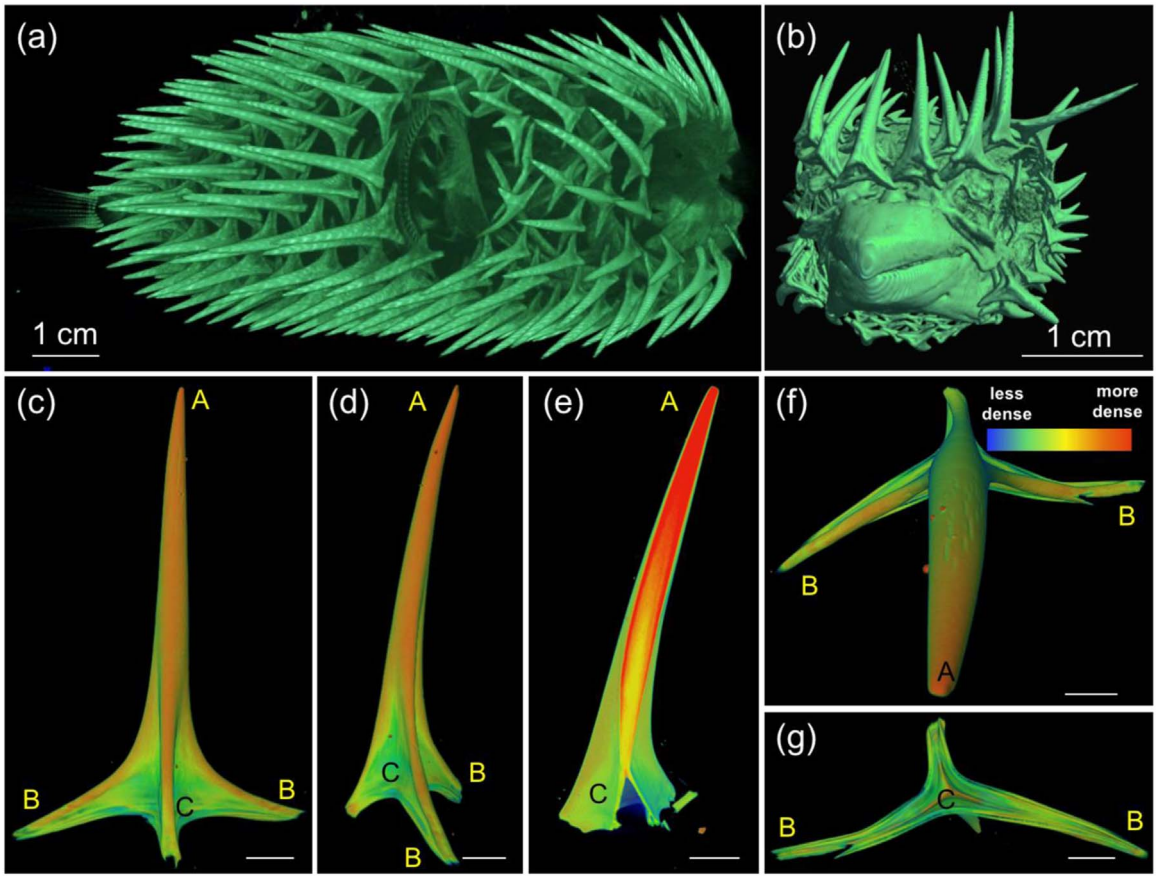

Fig. 7. X-ray microscopy images of *D. holocanthus*: (a) lateral and (b) anterior view. X-ray microscopy images of *D. holocanthus* spine: (c) anterior view, (d) left lateral view, (e) longitudinal cross-section, (f) dorsal view, and (g) ventral view. Unlabeled scale bars are 500 μm. Spine coloration represents density of the sample. Red symbolizes regions of highest density and blue represents regions of lowest density. The anterior view and left lateral view of the spines show different sections A, B, and C of the spine (defined in Fig. 3).

Putting together all the microstructural information, it can be seen that the spine (*D. holocanthus*), which is ~10 mm long and ~ 1 mm in diameter, has the structure described in Fig. 11. In the longitudinal direction, mineralized collagen strips are connected by mineralized bridges to form radially aligned sheets (shown in orange) of thickness ~2 μm. Alternating between the mineralized collagen sheets are unmineralized collagen fibril layers with thicknesses of ~0.5 μm that are oriented orthogonally with respect to the mineralized, fibrillar sheets and are radially aligned (shown in green). In the transverse cross-section, there are concentric growth rings of 2 to 7.5 μm widths. The radial and concentric structures observed in the spine cross-sections may benefit the spines mechanically by deflecting cracks and strengthening the spine during bending.

3.3. Mechanical properties

Nanoindentation was performed on the longitudinal cross-section of the *D. holocanthus* spinous process. The Young's modulus and hardness values were calculated with the values from the force-displacement curves of each indent using the Oliver-Pharr method (Oliver and Pharr, 1992). Surrounding the spine is epoxy with a Young's modulus of 3.13 ± 0.22 GPa and hardness of 0.208 ± 0.02 GPa. It has been shown previously in bone that embedding indentation samples in epoxy results in a minor increase in hardness (Evans et al., 1990; Hoffler et al., 2005) and little to no difference in Young's modulus (Hoffler et al., 2005; Zysset, 2009).

Young's modulus and hardness maps (Fig. 12) demonstrate that the spines have a stiffness and hardness gradient across the spinous process. Young's modulus of the spine was found to range from 6.8 to 20.5 GPa and the hardness ranged between 290 to 820 MPa. Multiple linear regression analysis performed on nanoindentation data found that the distance along the spine from the base, radial distance from the spine center, and their interaction are significant predictors of Young's modulus with $p < 0.0005$, $p=0.020$, and $p=0.019$, respectively. For hardness, only distance along the spine was a statistically significant predictor with $p < 0.0005$. These results confirm that the spine is a functionally graded material where the outside of the spine as well as the region near the tip is stiffer and harder than the rest of the spine. Revisiting the XRM images of the spine cross-section (Fig. 7e), one can see that higher density implies greater mineralization, which results in higher stiffness and hardness. A gradient in mechanical properties increases interfacial toughness and prevents failure between materials of different moduli (Bruet et al., 2008; Miserez et al., 2008). In the case of the spider fang, the stiffening of the fang near the tip is used to reinforce the fang at the location of maximum stress (Bar-On et al., 2014). The porcupine fish spine likely employs both strategies using material property gradient to prevent failure.

3.4. Modeling mechanical behavior and mechanical tests

Mechanical models were developed and used to calculate maximum tensile strength, maximum strain, and Young's modulus for spines tested using a cantilever beam test. Two models of the porcupine fish spine are compared: the spine as a uniform cylindrical beam and the spine as a tapered beam with a circular cross-section (both shown in Fig. 13) that better represents the shape of the spine. While some curvature is observed in the spine (Fig. 7d), linear tapering was assumed based on Fig. 7c for simplification of the mathematical model. P is a point load at the end of the beam, L is the length of the beam, d is the diameter of the cylindrical beam, d_B is the larger diameter of the

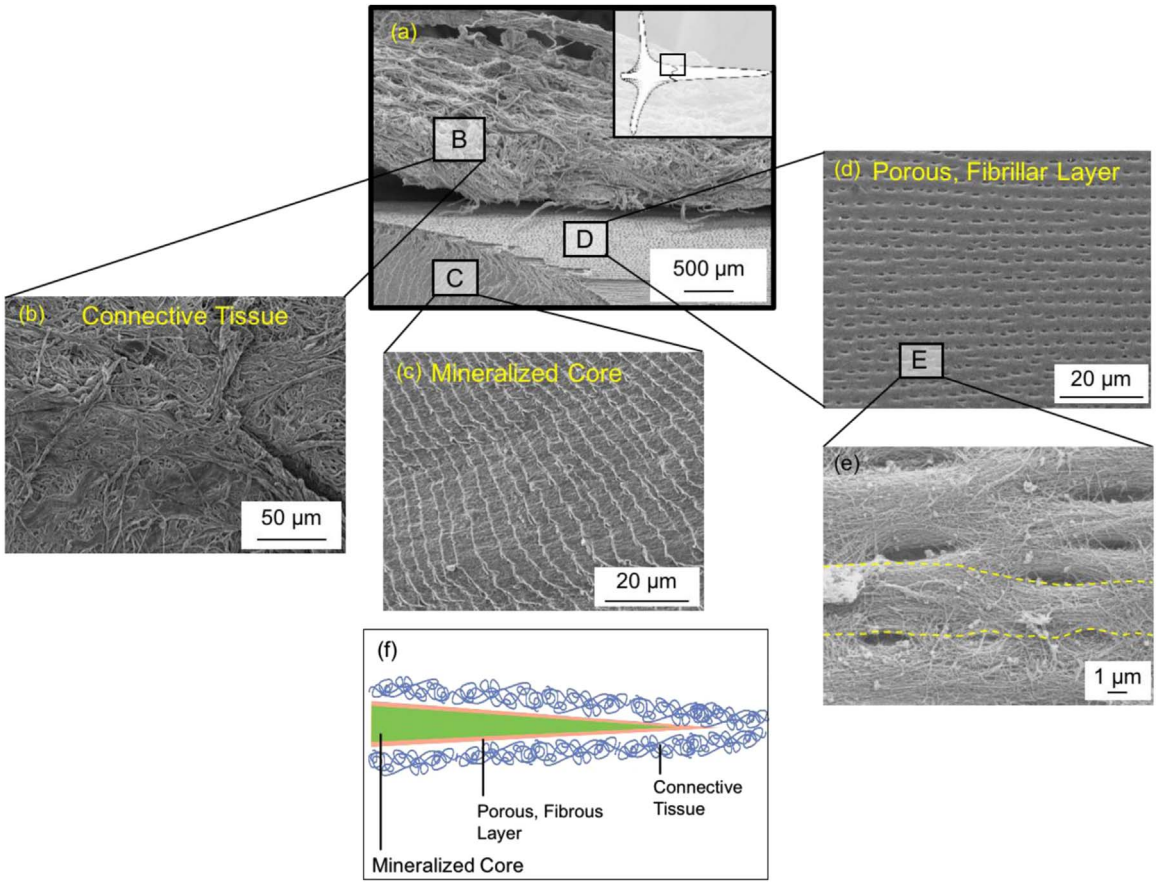

Fig. 8. Scanning electron micrograph of freeze-fractured *D. hystrix* spine layered structure. (a) Surface of the spine (distal end pointing right) shows the layers that make up the spine. Inset image shows location on spine where sample was fractured. The boxed areas in (a) correspond to images shown in (b), (c) and (d). (b) Connective tissue, (c) mineralized core, and (d) porous, fibrillar layer. (e) Boxed region (E) in (d) and shows the fibrils that make up the fibrillar strips (outlined by yellow dotted lines) seen in (d). (f) Overall schematic diagram of the layers in the spine.

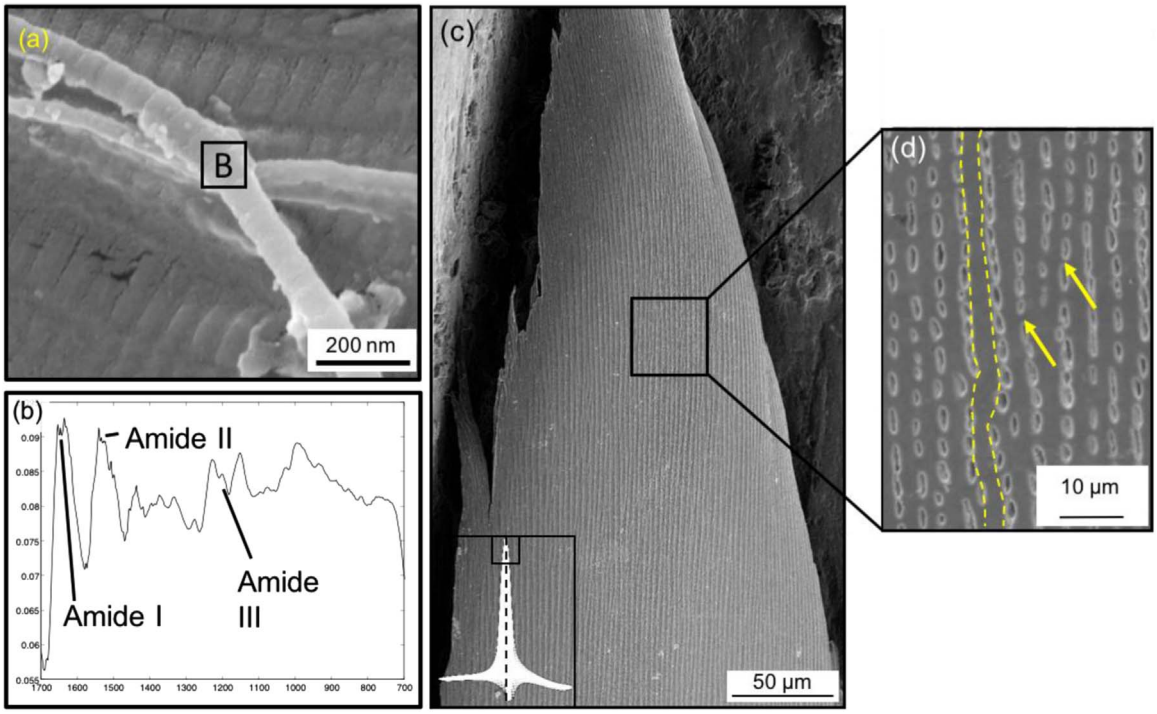

Fig. 9. (a) Scanning electron microscopy image of banded fibrils located in the spine base of *D. holocanthus*. The banded structure is indicative of collagen. The boxed region (B) in (a) is the collagen for which the Fourier transform infrared spectrum is shown in (b). Scanning electron micrographs of the *D. holocanthus* spine structure. (c) Longitudinal cross-section of spine showing longitudinal alignment. The inset diagram shows where spine was cut (along dotted line) and location on spine that image was taken (boxed area). (d) Deproteinized spine showing mineralized strips (outlined by yellow dotted line) and mineralized bridges (indicated by yellow arrows) between them.

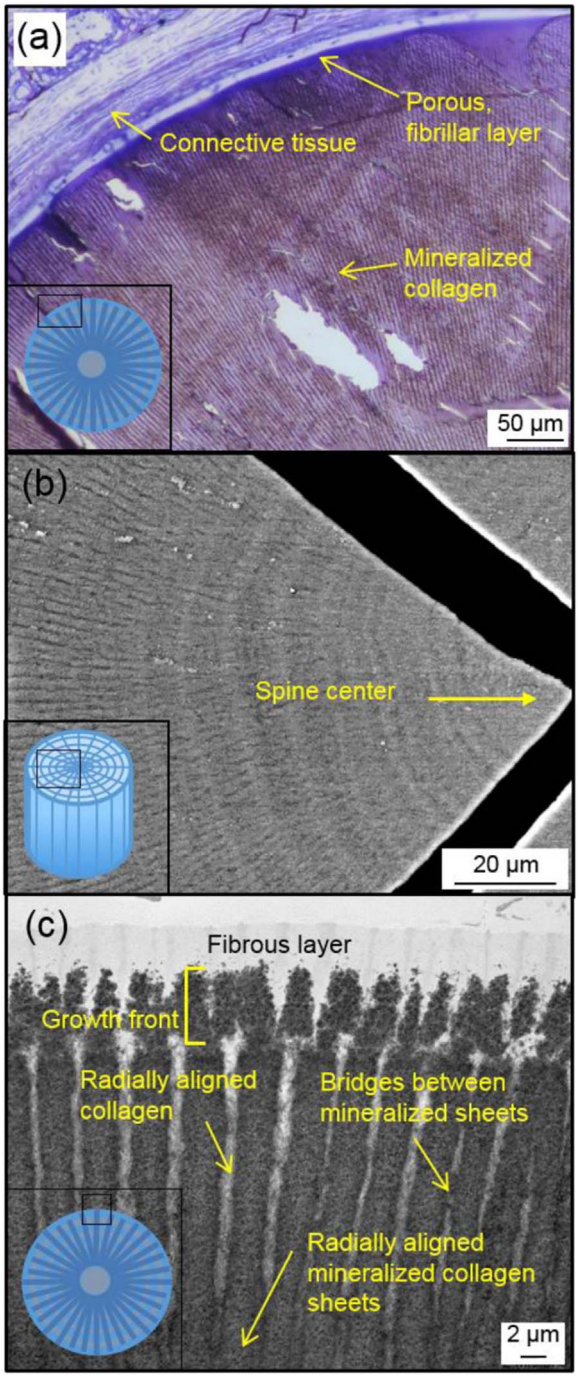

Fig. 10. (a) Light microscopy image of a spine cross-section that was embedded in epoxy and stained with toluidine blue with schematic diagram of the *D. hystrix* spine transverse cross-section (inset). (b) Back-scattered electron microscopy image of cross-section of a *D. hystrix* spine in section A (shown in Fig. 3). A radially aligned pattern and growth rings can be observed. Inset image shows transverse cross-section that the micrograph is taken from. (c) Transmission electron micrograph showing the transverse cross-section of a spine. Inset image shows the portion of the transverse cross-section that the micrograph is taken from. Dark columns are mineralized collagen embedded in a fibrillar matrix. Features pointed out using arrows include mineralized collagen bridges between mineralized sheets, radially aligned collagen, and radially aligned, mineralized collagen sheets. Bracket shows mineral growth front.

tapered beam, d_A is the smaller diameter of the tapered beam, and $\beta = d_A/d_B$ is the tapering ratio. Equations for the maximum tensile stress and strain and the Young's modulus for the two models are shown and derived in Supplementary Materials. In order to compare mechanical properties using the uniform beam and tapered beam models, a diameter d of the uniform cross-section beam was calculated by equating the volumes (V) of the two types of beams. Equations for solving for d are in Supplementary Materials.

After testing five *D. holocanthus* spine samples, the equations for the two different models were applied to the data. It can be observed from Table 3 that for an average tapering ratio β=0.21 ± 0.04, the average maximum tensile stresses are 612 ± 81 and 760 ± 286 MPa for the uniform and tapered beam models, respectively. The maximum tensile strengths are not significantly different (student t-test, p = 0.39). Young's modulus values are 12.9 ± 3.2 and 11.1 ± 3.4 GPa for uniform and tapered beam models, respectively, and are not significantly different (student t-test, p = 0.46), which are similar to the nanoindentation results (6.8–20.5 GPa). Strain at failure was found to increase significantly from 4.8 ± 0.4 to 6.8 ± 1% from the uniform beam to the tapered beam (student t-test, p = 0.011). The Young's moduli of both the tapered beam and the uniform cylindrical beam models also correspond well with values found in nanoindentation ($E \approx$ 6.8~20.5 GPa). Values from nanoindentation are likely higher than those calculated from mechanical tests, since the nanoindented samples were dried and cantilever test samples were hydrated. It is well known that dehydrated samples have higher stiffness (Nyman et al., 2006).

Fig. 14 demonstrates the relationship between stress in the uniform beam and in the tapered beam with respect to distance from the base. Lines with the same color represent models with the same volume for a certain β value, while the shaded region shows the range of stress for actual values of beta in the porcupine fish spine. For an average spine length, base diameter, and maximum load applied, β=0.2 results in similar maximum stress values between the two models. Observing only the tapered beam model, decreasing β increases the maximum tensile stress and shifts the location of the maximum stress toward the tip of the spine; increasing β decreases the maximum tensile stress and shifts the location toward the base of the spine. Small changes in β result in large variations in maximum stress, which helps to explain the large standard deviation seen in the experimental results using the tapered beam analytical equation. Although the maximum stress is not significantly changed between the two models, the location of the maximum stress changes from the fixed end of the beam for a uniform cross-section beam to a distance close to the tip of the beam for a tapered beam. This may be beneficial so that if the spine in the porcupine fish does break, it breaks near the tip, and most of the spine material will be conserved. This structural function has also been observed in the spider fang, which also has a tapered structure and stiffness gradient (Bar-On et al., 2014).

4. Applications and bioinspiration

Bioinspiration is a field that aims to study designs in nature that have been developing for millions of years through evolution and use them to inspire human engineering applications. In recent years, bioinspiration has been gaining more attention. Scales in particular have been studied extensively because they help protect an animal while still maintaining flexibility and mobility (Long et al., 1996; Zhu et al., 2012). The erectile spines of the porcupine fish increase the size of the fish, making the fish difficult for predators to swallow, but allow the fish to become streamlined and smooth when not being attacked. These spines also serve to irritate the predator with their sharp tapered ends while being lightweight, allowing the porcupine fish to stay buoyant.

Many researchers who study spine structures argue that the design of the spines can be used for biomedical applications such as more efficient needles. However, many of the spines studied, such as those of the stingray, bee, and cactus, have serrated or barbed edges. This design makes it easy for spines to penetrate the skin, but difficult to take out and are meant to inflict as much damage as possible to deter predators. While the spines of the porcupine fish do not have serrated

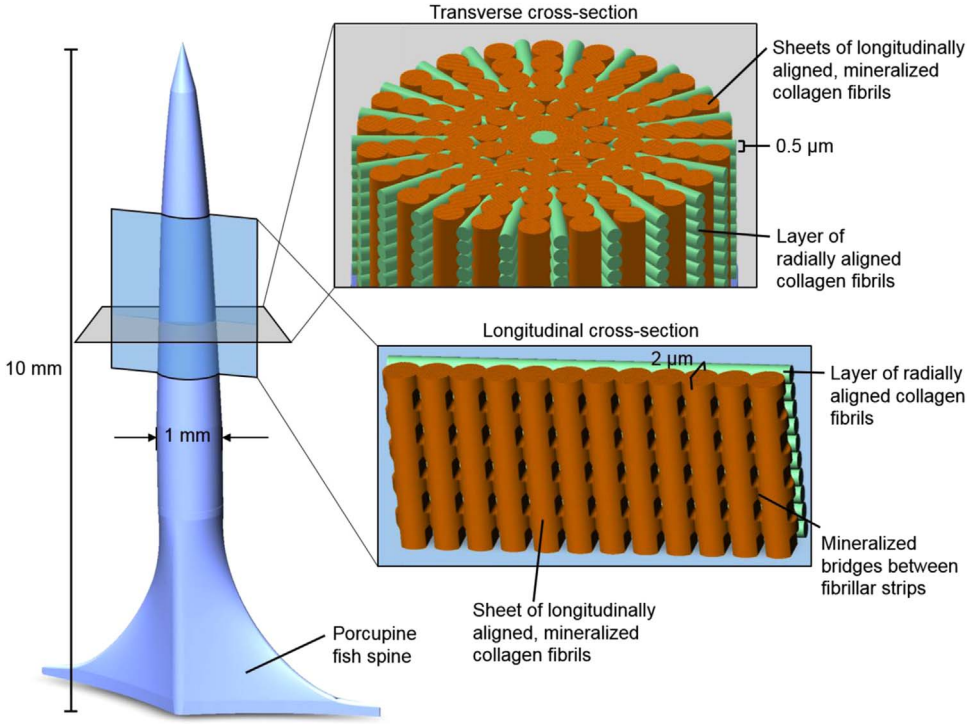

Fig. 11. Schematic diagram of the hierarchical structure of a porcupine fish spine showing the orientation of the mineralized fibrillar sheets and layers of radially aligned collagen fibrils. Orange color represents sheets of longitudinally aligned, mineralized collagen fibrils, green color represents sheets of radially aligned collagen fibrils that are not mineralized, and the blue color represents outer surface of the spine. Concentric growth rings form in the transverse cross-section. Diagram courtesy of S.E. Naleway.

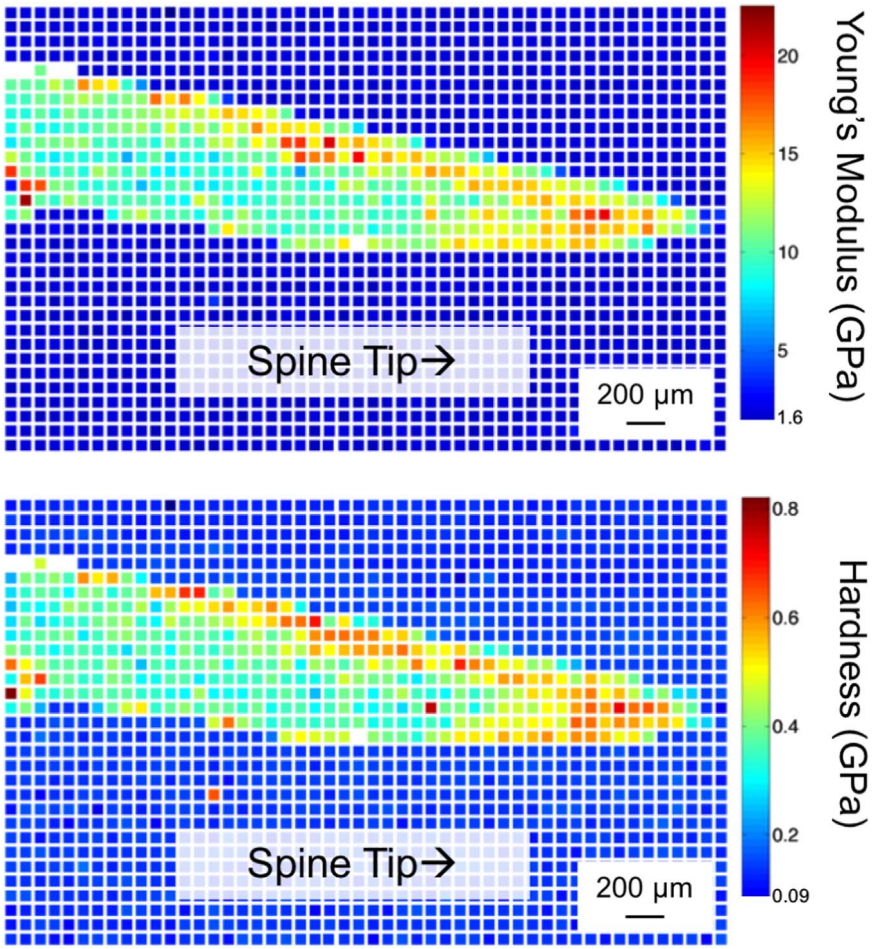

Fig. 12. Nanoindentation map for the spinous process (Fig. 3).

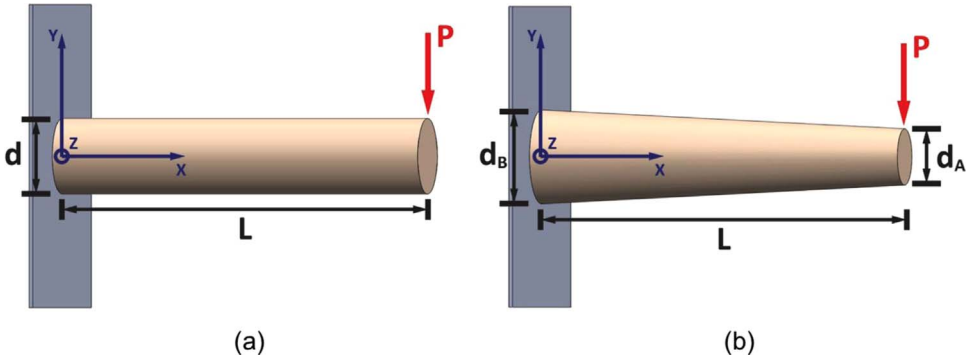

Fig. 13. (a) Uniform cylindrical cantilever beam with a constant diameter d. (b) Tapered cylindrical cantilever beam, where d_B is the larger diameter, d_A is the smaller diameter. L is beam length and P is the point load at the end of the beam for both models. Diagram courtesy of S.E. Naleway.

Table 3
Comparison of mechanical properties of the *D. holocanthus* spine from cantilever tests, calculated using the cylindrical beam model and the tapered circular beam model. Values are given as average ± standard deviation.

Mechanical property	Uniform beam	Tapered beam
Maximum tensile stress (MPa)	612 ± 81	760 ± 286
Young's modulus (GPa)	12.9 ± 3.2	11.1 ± 3.4
Strain at failure (%)	4.8 ± 0.4	6.8 ± 1

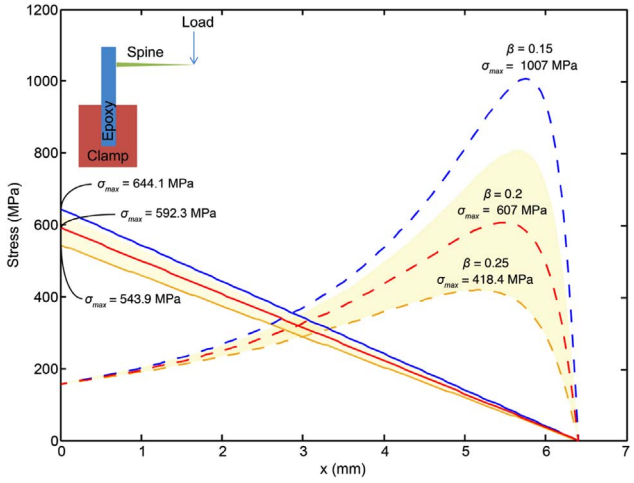

Fig. 14. Calculated maximum stress at the beam top surface as a function of x from 0 to the length of the beam L. Solid line graphs indicate the uniform cylinder model, while dotted line graphs are for the tapered cylinder models with β values shown on the graph. Matching colors indicate models with the same volumes based on the corresponding β values. Shaded regions represent values based on the average and standard deviation of β in the porcupine fish spine. Values used for P, L, d_B, and β are averages from experiments. A schematic of the spine cantilever beam test is shown in the top left corner.

edges, they are meant to pierce predators that attempt to eat them. Instead of considering these spines for needle applications, it may be more worthwhile to study the spines for their resistance to breakage as well as their ability to act as a deployable defense that can be compacted after use. In fact, porcupine fish spines have already been used for helmets in Polynesian island natives to defend against weapons made of shark teeth (Gudger, 1930), as shown in Fig. 15.

5. Conclusions

The structure, composition, and mechanical properties of the porcupine fish spines from *Diodon holocanthus* and *Diodon hystrix* were explored for the first time. There were no striking differences between the morphology of the spines of the two species. X-ray diffraction (XRD), energy dispersive X-ray spectroscopy (EDS), and thermogravimetric analysis (TGA), were used to determine the composition of the spine. Micro- and nano-computed tomography (CT), light microscopy, scanning electron microscopy (SEM), and transmission electron microscopy (TEM) were used to observe the macro- and microstructure of the spine. Mechanical properties were assessed using both nanoindentation and a cantilever beam test. The major findings are:

Fig. 15. Porcupine fish helmet created by Gilbert Island Natives (Pitt Rivers Museum).

- *D. holocanthus* and *D. hystrix* specimens had body lengths of ~9 cm and ~19 cm, respectively. *D. holocanthus* spines, for which mechanical testing was done were ~10 mm in length and ~1 mm in diameter.
- Spines of both species contain different ratios of mineral, protein, and water in different sections of the spine. The spinous process is the most mineralized, the lateral processes were less mineralized, and the spine base, which includes the axial process, was the least mineralized. The mineral component is nanocrystalline hydroxyapatite with crystallite sizes of ~20 nm and the protein component is collagen.
- The spine is composed of multiple layers with an intricate microstructure with four main layers from deep to superficial: a miner-

alized core, a porous fibrillar layer, a layer of connective tissue, and a layer of skin that is outside of the connective tissue.

- The spine is composed of radially aligned sheets of longitudinally aligned, mineralized, collagen fibrils. In between these sheets are layers of radially aligned collagen fibrils. The spine also has concentric growth rings in the transverse cross-section.
- Nanoindentation showed that the spine has a Young's modulus that ranges from 6.7 to 20. 4 GPa and a hardness that ranges from 291 to 821 MPa along the spine length. Gradients in Young's modulus and hardness were found in the longitudinal direction of spinous process, and the distal region of the spine was stiffer and harder than the remainder of the spine.
- Cantilever beam tests were performed and a mathematical model for a tapered beam (spine) was compared to that of a uniform beam. The comparison showed that while the maximum stress and Young's modulus of the two configurations were not significantly different, the location of the maximum stress for the tapered beam is near the tip of the spine rather than at the spine base, which is the maximum stress location for a uniform beam. The tapering is beneficial so that if a spine breaks, it breaks at the tip, thus preserving the majority of the spine.

Acknowledgements

This work was supported by a Multi-University Research Initiative through the Air Force Office of Scientific Research (AFOSR-FA9550-15-1–0009), a National Science Foundation grant (1507978), and a National Institutes of Health grant (P41GM103412). We thank Professor Philip Hastings and H.J. Walker of the Scripps Institution of Oceanography for generously providing the fish samples; Andrea Thor, Mason Mackey, and Professor Mark Ellisman from the National Center for Microscopy and Imaging at UC San Diego for assisting with sample sectioning and techniques for electron microscopy; Dr. Katya Novitskaya for performing XRD; Esther Cory and Professor Robert Sah for performing the μ-CT scans; Dr. James Tyler of the Smithsonian Institution for insight into the phylogeny and anatomy of porcupine fish; and Professor Steven Naleway for assistance with designing figures.

Appendix A. Supporting information

Supplementary data associated with this article can be found in the online version at doi:10.1016/j.jmbbm.2017.02.029.

References

Aquarium of the Pacific, 2015. Balloonfish (Spiny Porcupine Fish), Aquarium of the Pacific.
Bar-On, B., Barth, F.G., Fratzl, P., Politi, Y., 2014. Multiscale structural gradients enhance the biomechanical functionality of the spider fang. Nat. Commun. 5, 3894.
Bassett, H., 1917. LVI.—The phosphates of calcium. Part IV. The basic phosphates. J Chem. Soc. 111, 620–642.
Bechtle, S., Ang, S.F., Schneider, G.A., 2010. On the mechanical properties of hierarchically structured biological materials. Biomaterials 31, 6378–6385.
Berman, A., Addadi, L., Kvick, Å., Leiserowitz, L., Nelson, M., Weiner, S., 1990. Intercalation of sea urchin proteins in calcite: study of a crystalline composite material. Science 250, 664–667.
Bigi, A., Ripamonti, A., Cojazzi, G., Pizzuto, G., Roveri, N., Koch, M.H.J., 1991. Structural analysis of turkey tendon collagen upon removal of the inorganic phase. Int. J. Biol. Macromol. 13, 110–114.
Bowes, J.H., Murray, M.M., 1935. The chemical composition of teeth: the composition of human enamel and dentine. Biochem. J. 29, 2721.
Brainerd, E.L., 1994. Pufferfish inflation: functional morphology of postcranial structures in Diodon holocanthus (Tetraodontiformes). J. Morphol. 220, 243–261.
Bruet, B.J.F., Song, J., Boyce, M.C., Ortiz, C., 2008. Materials design principles of ancient fish armour. Nat. Mater. 7, 748–756.
Byeon, M.S., Park, J.Y., Yoon, S.W., Kang, H.W., 2011. Structure and development of spines over the skin surface of the river puffer Takifugu obscurus (Tetraodontidae, Teleostei) during larval growth. J. Appl. Ichthyol. 27, 67–72.
Chen, P.-Y., Toroian, D., Price, P.A., McKittrick, J., 2011. Minerals form a continuum phase in mature cancellous bone. Calcif. Tissue Int. 88, 351–361.
Chen, P.Y., McKittrick, J., 2011. Compressive mechanical properties of demineralized and deproteinized cancellous bone. J. Mech. Behav. Biomed. Mater. 4, 961–973.
Clarke, M.W., Irvine, S.B., 2006. Terminology for the ageing of chondrichthyan fish using dorsal-fin spines. Environ. Biol. Fish. 77, 273–277.
Corsi, G., Corsi, B., 2001. Pterois volitans, Red lionfish, CalPhotos.
de Albuquerque, C.Q., Martins, A.S., Leite, N.D., de Araujo, J.N., Ribeiro, A.M., 2011. Age and growth of the queen triggerfish Balistes vetula (Tetraodontiformes, Balistidae) of the central coast of Brazil. Braz. J. Oceanogr. 59, 231–239.
Ehrlich, H., 2015. Biological Materials of Marine Origin: Vertebrates. Springer.
Elliott, J.C., Mackie, P.E., Young, R.A., 1973. Monoclinic hydroxyapatite. Science 180, 1055–1057.
Evans, G., Behiri, J., Currey, J., Bonfield, W., 1990. Microhardness and Young's modulus in cortical bone exhibiting a wide range of mineral volume fractions, and in a bone analogue. J. Mater. Sci. Mater. Med. 1, 38–43.
Gindl-Altmutter, W., Keckes, J., 2012. The structure and mechanical properties of spines from the cactus Opuntia ficus-indica. Bioresources 7, 1232–1237.
Gudger, E.W., 1930. Helmets from skins of the porcupine-fish. Sci. Mon. 30, 432–442.
Halstead, B.W., Chitwood, M.J., Modglin, F.R., 1955. The anatomy of the venom apparatus of the zebrafish, Pterois-volitans (Linnaeus). Anat. Rec. 122, 317–334.
Halstead, B.W., Modglin, F.R., 1950. A preliminary report on the venom apparatus of the bat-ray, Holorhinus californicus. Copeia 1950, 165–175.
Hamada, M., Nagai, T., Kai, N., Tanoue, Y., Mae, H., Hashimoto, M., Miyoshi, K., Kumagai, H., Saeki, K., 1995. Inorganic constituents of bone of fish. Fish. Sci. 61, 517–520.
Hertwig, I., Eichelberg, H., Hentschel, J., 1992. Light and electron microscopic studies of the skin of the Palembang puffer, Tetraodon steindachneri (Teleostei, Tetraodontidae). Zoomorphology 111, 193–205.
Hoffler, C.E., Guo, X.E., Zysset, P.K., Goldstein, S.A., 2005. An application of nanoindentation technique to measure bone tissue lamellae properties. J. Biomech. Eng.-T ASME 127, 1046–1053.
Ikoma, T., Kobayashi, H., Tanaka, J., Walsh, D., Mann, S., 2003a. Microstructure, mechanical, and biomimetic properties of fish scales from Pagrus major. J. Struct. Biol. 142, 327–333.
Ikoma, T., Kobayashi, H., Tanaka, J., Walsh, D., Mann, S., 2003b. Physical properties of type I collagen extracted from fish scales of Pagrus major and Oreochromis niloticas. Int. J. Biol. Macromol. 32, 199–204.
Janković, B., Kolar-Anić, L., Smičiklas, I., Dimović, S., Aranđelović, D., 2009. The non-isothermal thermogravimetric tests of animal bones combustion. Part. I. Kinetic analysis. Thermochim. Acta 495, 129–138.
Leis, J.M., 1978. Systematics and zoogeography of porcupinefishes (Diodon, Diodontidae, Tetraodontiformes), with comments on egg and larval development. Fish. B-Noaa 76, 535–567.
Leis, J.M., 2006. Nomenclature and distribution of the species of the porcupinefish family Diodontidae (Pisces, Teleostei). Mem. Mus. Vic. 63, 77–90.
Lin, Y.S., Wei, C.T., Olevsky, E.A., Meyers, M.A., 2011. Mechanical properties and the laminate structure of Arapaima gigas scales. J Mech. Behav. Biomed. Mater. 4, 1145–1156.
Liu, Z.Q., Zhu, Y.K., Jiao, D., Weng, Z.Y., Zhang, Z.F., Ritchie, R.O., 2016. Enhanced protective role in materials with gradient structural orientations: lessons from Nature. Acta Biomater. 44, 31–40.
Long, J.H., Hale, M.E., McHenry, M.J., Westneat, M.W., 1996. Functions of fish skin: flexural stiffness and steady swimming of longnose gar Lepisosteus osseus. J. Exp. Biol. 199, 2139–2151.
Malainine, M.E., Dufresne, A., Dupeyre, D., Mahrouz, M., Vuong, R., Vignon, M.R., 2003. Structure and morphology of cladodes and spines of Opuntia ficus-indica. Cellulose extraction and characterisation. Carbohyd Polym. 51, 77–83.
Martin, T., Marugan-Lobon, J., Vullo, R., Martin-Abad, H., Luo, Z.-X., Buscalioni, A.D., 2015. A Cretaceous eutriconodont and integument evolution in early mammals. Nature 526, 380–384.
Meinke, D.K., Skinner, H.C.W., Thomson, K.S., 1979. X-ray diffraction of the calcified tissues in Polypterus. Calcif. Tissue Int. 28, 37–42.
Miserez, A., Schneberk, T., Sun, C.J., Zok, F.W., Waite, J.H., 2008. The transition from stiff to compliant materials in squid beaks. Science 319, 1816–1819.
Moureaux, C., Perez-Huerta, A., Compere, P., Zhu, W., Leloup, T., Cusack, M., Dubois, P., 2010. Structure, composition and mechanical relations to function in sea urchin spine. J. Struct. Biol. 170, 41–49.
Nyman, J.S., Roy, A., Shen, X., Acuna, R.L., Tyler, J.H., Wang, X., 2006. The influence of water removal on the strength and toughness of cortical bone. J. Biomech. 39, 931–938.
Ocampo, R.R., Halstead, B.W., Modglin, F.R., 1953. The microscopic anatomy of the caudal appendage of the spotted eagleray, Aëtobatus narinari (Euphrasen), with special reference to the venom apparatus. Anat. Rec. 115, 87–99.
Oliver, W.C., Pharr, G.M., 1992. An improved technique for determining hardness and elastic-modulus using load and displacement sensing indentation experiments. J Mater. Res 7, 1564–1583.
Pedroso, C.M., Jared, C., Charvet-Almeida, P., Almeida, M.P., Neto, D.G., Lira, M.S., Haddad, V., Barbaro, K.C., 2007. Morphological characterization of the venom secretory epidermal cells in the stinger of marine and freshwater stingrays. Toxicon 50, 688–697.
Pitt Rivers Museum, Porcupine fish helmet, in: Pitt Rivers Museum (Ed.), Arms and Armour: Selected Objects from the Upper Gallery, ⟨http://web.prm.ox.ac.uk/weapons/index.php/tour-by-region/oceania/oceania/arms-and-armour-oceania-193/⟩.
Pompe, W., Worch, H., Epple, M., Friess, W., Gelinsky, M., Greil, P., Hempel, U., Scharnweber, D., Schulte, K., 2003. Functionally graded materials for biomedical applications. Mat. Sci. Eng. A-Struct. 362, 40–60.

Prado, J.m., Béarez, P., Ibarra Santacruz, A.N., 2004. Peces marinos del Ecuador continental.
Reddy, G., 2006. Scale structure of a cobitid fish, Cobitis linea (Heckel, 1849) using different modes of SEM. Curr. Sci. 91, 1464.
Rignanese, L., 2005. Opuntia ficus-indica; Indian-fig.
Sanches, J.G., 1991. Catálogo dos principais peixes marinhos da República da Guiné-Bissau.
Santini, F., Sorenson, L., Alfaro, M.E., 2013. A new phylogeny of tetraodontiform fishes (Tetraodontiformes, Acanthomorpha) based on 22 loci. Mol. Phylogenet Evol. 69, 177–187.
Sire, J.Y., Donoghue, P.C.J., Vickaryous, M.K., 2009. Origin and evolution of the integumentary skeleton in non-tetrapod vertebrates. J. Anat. 214, 409–440.
Su, X., Kamat, S., Heuer, A.H., 2000. The structure of sea urchin spines, large biogenic single crystals of calcite. J. Mater. Sci. 35, 5545–5551.
Tonge, S.J., 2013. Tachyglossus aculeatus setosus, Tasmanian Echidna, CalPhotos.
Tonge, S.J., 2014. Hystrix cristata, Crested Porcupine, CalPhotos.
Urist, M.R., 1961. Calcium and phosphorus in the blood and skeleton of the Elasmobranchii. Endocrinology 69, 778–801.
Vidal, B.D., Mello, M.L.S., 2011. Collagen type I amide I band infrared spectroscopy. Micron 42, 283–289.
Vincent, J.F.V., Owers, P., 1986. Mechanical design of hedgehog spines and porcupine quills. J. Zool. 210, 55–75.
Zhao, Z.-L., Shu, T., Feng, X.-Q., 2016. Study of biomechanical, anatomical, and physiological properties of scorpion stingers for developing biomimetic materials. Mat. Sci. Eng. C 58, 1112–1121.
Zhao, Z.-L., Zhao, H.-P., Ma, G.-J., Wu, C.-W., Yang, K., Feng, X.-Q., 2015. Structures, properties, and functions of the stings of honey bees and paper wasps: a comparative study. Biol. Open, Biol., 012195.
Zhu, D.J., Ortega, C.F., Motamedi, R., Szewciw, L., Vernerey, F., Barthelat, F., 2012. Structure and mechanical performance of a "modern" fish scale. Adv. Eng. Mater. 14, B185–B194.
Zylberberg, L., Bonaventure, J., Cohensolal, L., Hartmann, D.J., Bereiterhahn, J., 1992. Organization and characterization of fibrillar collagens in fish scales in situ and in vitro. J. Cell Sci. 103, 273–285.
Zylberberg, L., Nicolas, G., 1982. Ultrastructure of scales in a teleost (Carassius-auratus L.) after use of rapid freeze-fixation and freeze-substitution. Cell Tissue Res. 223, 349–367.
Zysset, P.K., 2009. Indentation of bone tissue: a short review. Osteoporos. Int. 20, 1049–1055.